nature cell biology

SUPPLEMENTARY INFORMATION

https://doi.org/10.1038/s41556-018-0174-4

In the format provided by the authors and unedited.

m^{6}A mRNA methylation regulates AKT activity to promote the proliferation and tumorigenicity of endometrial cancer

Jun Liu[1,2,12], Mark A. Eckert[3,12], Bryan T. Harada[1,2,12], Song-Mei Liu[4,12], Zhike Lu[1,2], Kangkang Yu[1,2,5], Samantha M. Tienda[3], Agnieszka Chryplewicz[3], Allen C. Zhu[1,2,6], Ying Yang[4], Jing-Tao Huang[4], Shao-Min Chen[4], Zhi-Gao Xu[7], Xiao-Hua Leng[8], Xue-Chen Yu[9], Jie Cao[10], Zezhou Zhang[10], Jianzhao Liu[10], Ernst Lengyel[3]* and Chuan He[1,2,11]*

[1]Department of Chemistry and Institute for Biophysical Dynamics, The University of Chicago, Chicago, IL, USA. [2]Howard Hughes Medical Institute, Chicago, IL, USA. [3]Department of Obstetrics and Gynecology/Section of Gynecologic Oncology, The University of Chicago, Chicago, IL, USA. [4]Center for Gene Diagnosis, Zhongnan Hospital of Wuhan University, Wuhan, China. [5]College of Chemistry, Sichuan University, Chengdu, China. [6]Committee on Cancer Biology and Medical Scientist Training Program, The University of Chicago, Chicago, IL, USA. [7]Department of Pathology, Zhongnan Hospital of Wuhan University, Wuhan, China. [8]Hubei Key Laboratory of Tumor Biological Behaviors & Hubei Cancer Clinical Study Center, Zhongnan Hospital of Wuhan University, Wuhan, China. [9]Department of Obstetrics and Gynecology, Zhongnan Hospital of Wuhan University, Wuhan, China. [10]MOE Key Laboratory of Macromolecular Synthesis and Functionalization, Department of Polymer Science and Engineering, Zhejiang University, Hangzhou, China. [11]Department of Biochemistry and Molecular Biology, The University of Chicago, Chicago, IL, USA. [12]These authors contributed equally: Jun Liu, Mark A. Eckert, Bryan T. Harada, Song-Mei Liu. *e-mail: elengyel@uchicago.edu; chuanhe@uchicago.edu

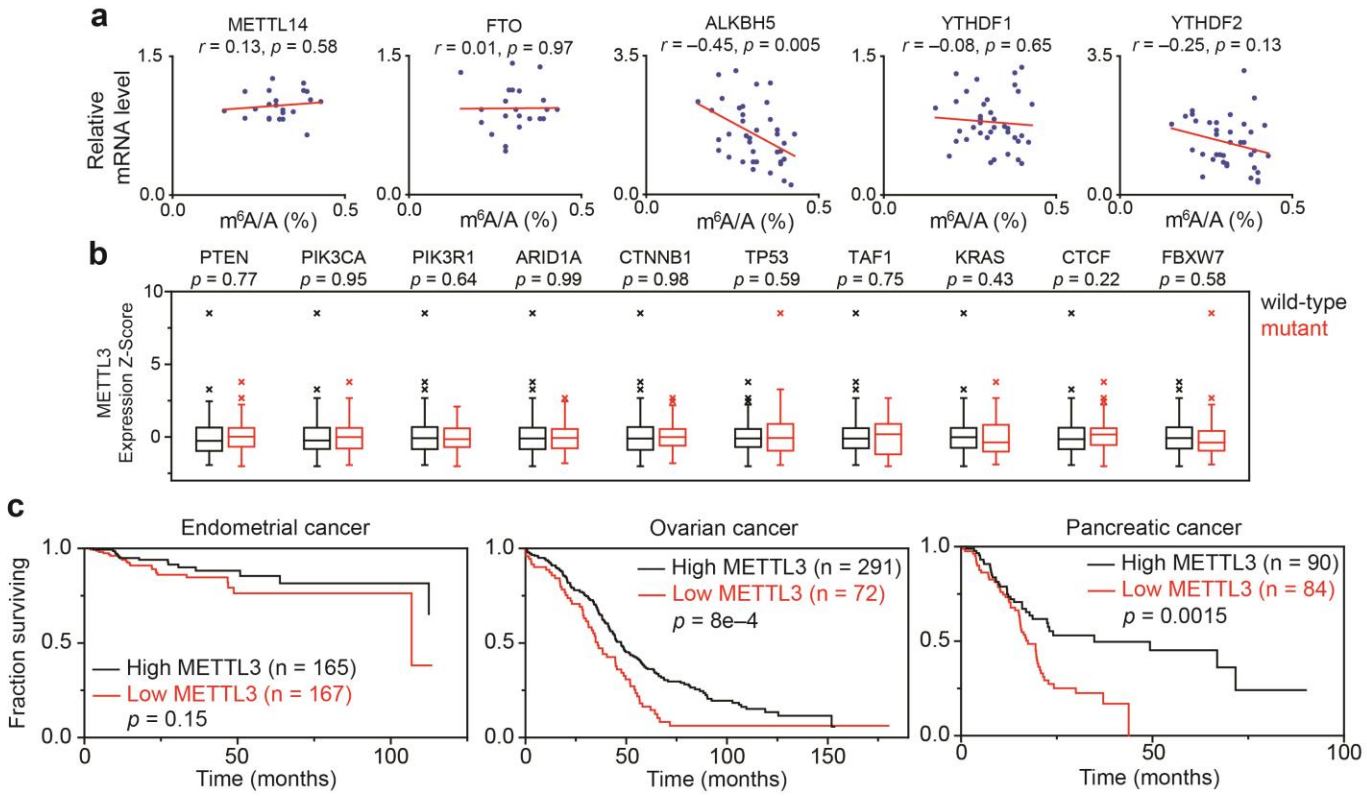

Supplementary Figure 1

Expression of m^{6}A-regulatory genes in endometrial cancer patients.

(**a**) Scatter plots showing the correlation of m^{6}A methylation levels with the expression of m^{6}A writers, erasers and readers in tumor tissue. Linear least squares line is shown in red. The Pearson correlation coefficient (*r*) and *p*-value (*p*) from a two-tailed *t*-test of $r = 0$ are shown. $n = 22$ tumor-normal pairs for FTO and METTL14, $n = 38$ tumor-normal pairs for the others. (**b**) Box plots showing the expression of METTL3 in TCGA endometrial cancer patients with tumors wild-type for (black) or containing mutations in (red) the indicated genes. *p*-values were calculated by two-tailed *t*-test. $n = 232$ tumors. For the box plots, the center line represents the median, the box limits show the upper and lower quartiles, whiskers represent 1.5x the interquartile range, and outliers are represented as individual data points. (**c**) Survival curves showing the correlation between METTL3 expression and patient overall survival in the TCGA datasets for endometrial cancer, high grade serous ovarian cancer, and pancreatic adenocarcinoma. *n* indicates the number of patients in each group. *p*-values were calculated by two-tailed log-rank test.

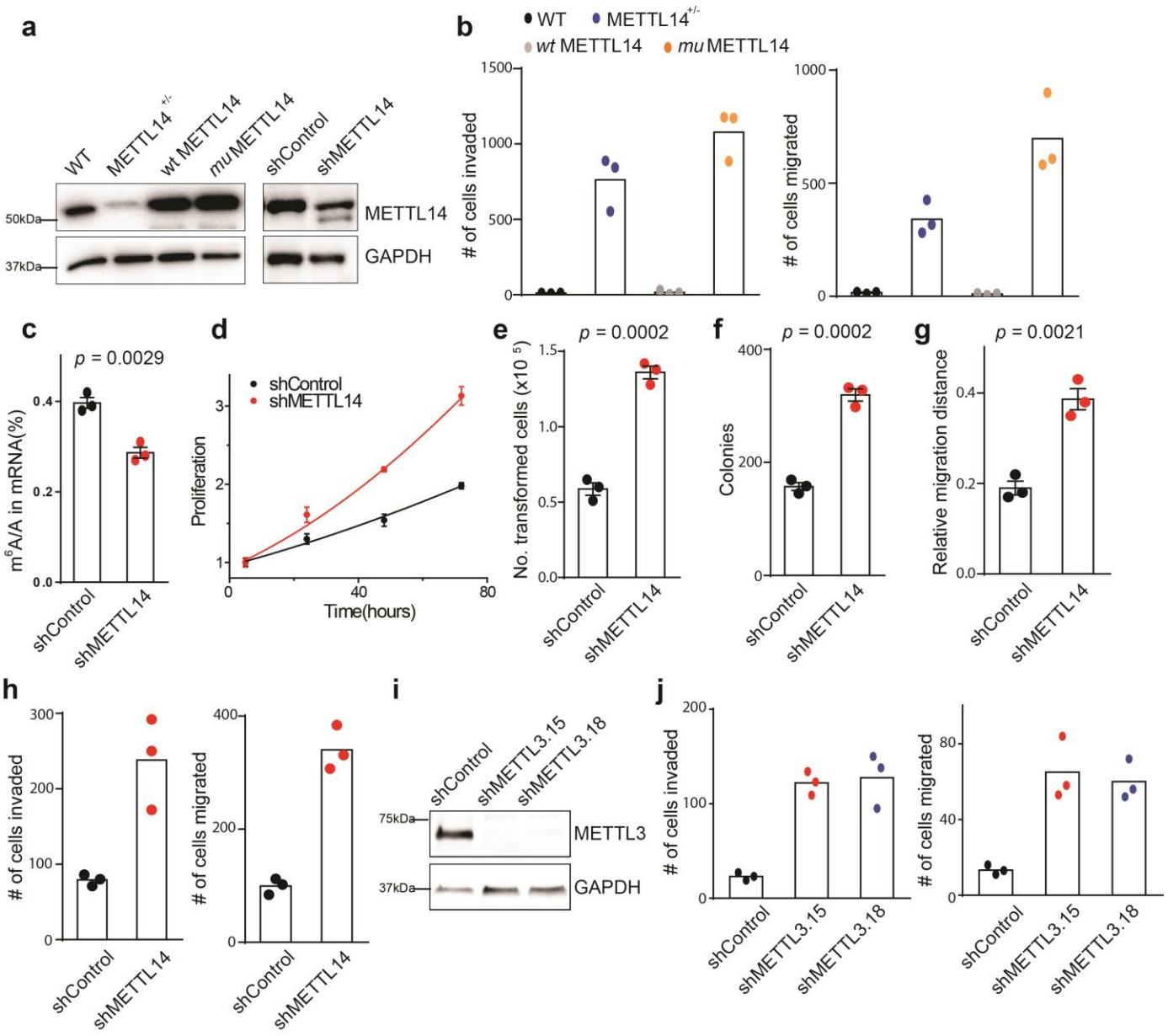

Supplementary Figure 2

Effects of alterations to m^{6}A mRNA methylation on the HEC-1-A endometrial cancer cell line.

(a) Immunoblot showing expression levels of the METTL14 in the wild-type HEC-1-A cell line, the METTL14$^{+/-}$ knockout cell line, knockout cells rescued with stable expression of wild-type and mutant METTL14, and HEC-1-A cells stably transfected with control shRNA or shRNA targeting METTL14. Three independent experiments have been repeated with similar results. (**b**) Transwell invasion and migration were assessed for wild-type HEC-1A cells, METTL14$^{+/-}$ knockout cells, and knockout cells rescued with wild-type or mutant METL14. (**c**) LC-MS/MS quantification of the m^{6}A/A ratio from polyA-RNA purified from the METTL14 knockdown and control cells. (**d-h**) Cell proliferation in an MTS assay (**d**), anchorage-independent cell growth (**e**), colony formation (**f**), migration in a wound healing assay (**g**), and transwell invasion and migration (**h**) of HEC-1-A cells expressing control shRNA or shRNA targeting METTL14. (**i**) Immunoblot showing the expression of METTL3 in HEC-1-A cells expressing a control shRNA or two different shRNAs targeting METTL3. Three independent experiments have been repeated with similar results. (**j**) Transwell invasion and migration were assessed for HEC-1A cells stably expressing control shRNA or shRNA targeting METTL3. For panels c-g , *n* = 3 biological replicates. Error bars indicate mean ± s.e.m. *p*-values determined by two-tailed *t*-test. For panel b, h and j, the bar shows the mean from *n* = 3 technical replicates. Raw gel images for panels a and i are provided in **Supplementary Fig. 8**.

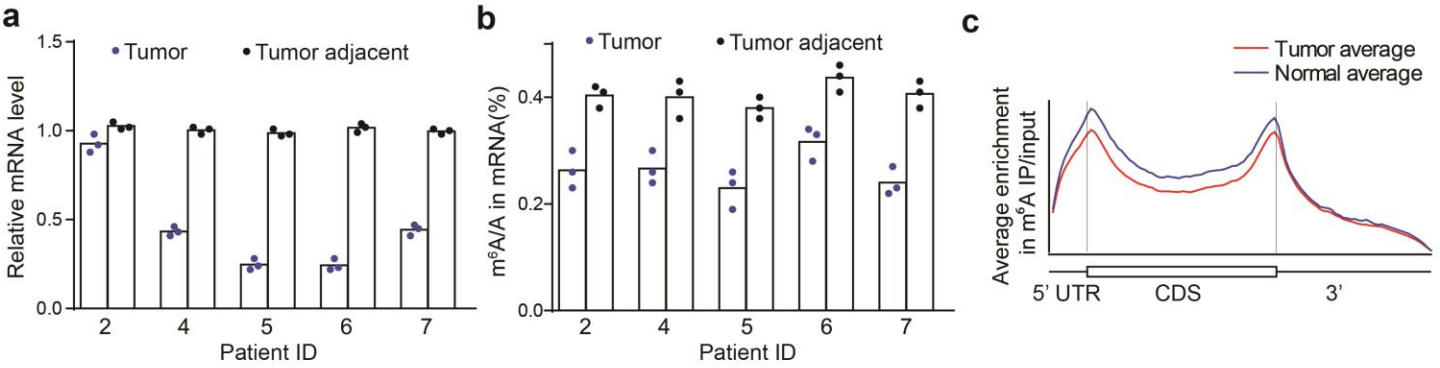

d

Rank	Tumor	Tumor adjacent
1		
2		
3		

e

Sample	Peaks	Genes	Patient 2	Patient 4	Patient 5	Patient 6	Patient 7	shControl	wt METTL14
			2000	10468	3561	10802	11286	9552	8904
Patient 2 (mu METTL14)	5634	2000							
Patient 4 (low METTL3)	29193	10468	1762						
Patient 5 (low METTL3)	6170	3561	750	3152					
Patient 6 (low METTL3)	32898	10802	1851	9162	3146				
Patient 7 (low METTL3)	31719	11286	1848	9509	3215	10259			
HEC-1-A shControl	29466	9552	1684	8112	2803	8317	8492		
HEC-1-A *wt* METTL14	22789	8904	1520	7608	2641	7864	8004	8165	

f

Sample	Patient 2	Patient 4	Patient 5	Patient 6	Patient 7	shMETTL3	*mu* METTL14
Patient 2							
Patient 4	0.475						
Patient 5	0.419	0.420					
Patient 6	0.308	0.430	0.288				
Patient 7	0.181	0.259	0.193	0.302			
HEC-1-A shMETTL3	0.353	0.402	0.308	0.348	0.233		
HEC-1-A *mu* METTL14	0.157	0.196	0.182	0.215	0.170	0.168	

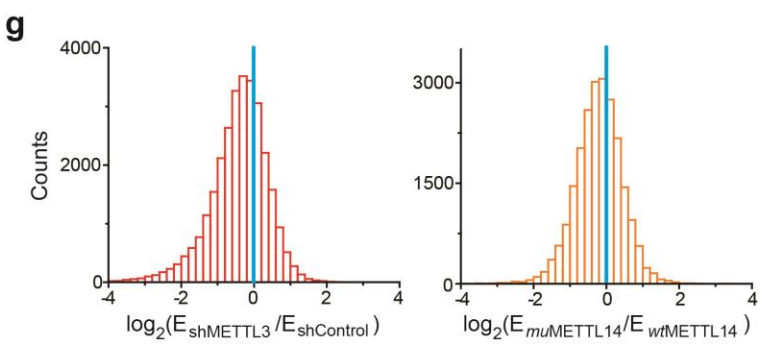

Supplementary Figure 3

m^{6}A-seq of endometrial tumors and cell lines.

(**a**) Relative expression of METTL3 in tumor and tumor-adjacent samples were measured by RT-qPCR. The bar shows the mean from from *n* = 3 technical replicates, (**b**) m^{6}A/A ratio of polyA-RNAs isolated from tumor and tumor-adjacent samples were measured by LC-MS/MS. The bar shows the mean from *n* = 3 technical replicates. (**c**) Metagene plots showing the average distribution of m^{6}A peaks identified across all transcripts in the tumor and tumor-adjacent samples from 5 patients. (**d**) Sequence logo showing the top motifs enriched across all m^{6}A-peaks identified from *n* = 5 patients. (**e**) The number of significant m^{6}A peaks detected and the number of transcripts containing a significant m^{6}A peak are reported. The number of genes containing a significant m^{6}A peak in each pair of samples is reported in the table. (**f**) For each pair of samples, we identified the set of transcripts showing a significant m^{6}A peak in both normal tissue samples. We then calculated the fraction of these transcripts showing a > 2-fold decrease in enrichment in both tumor samples and divided by all transcripts showing a > 2-fold decrease in enrichment in at least one tumor sample. (**g**) Histograms showing the changes in m^{6}A enrichment in the METTL3 knockdown versus control HEC-1-A cells (left) or mutant METTL14(R298P) versus wild-type METTL14 HEC-1-A cells (right).

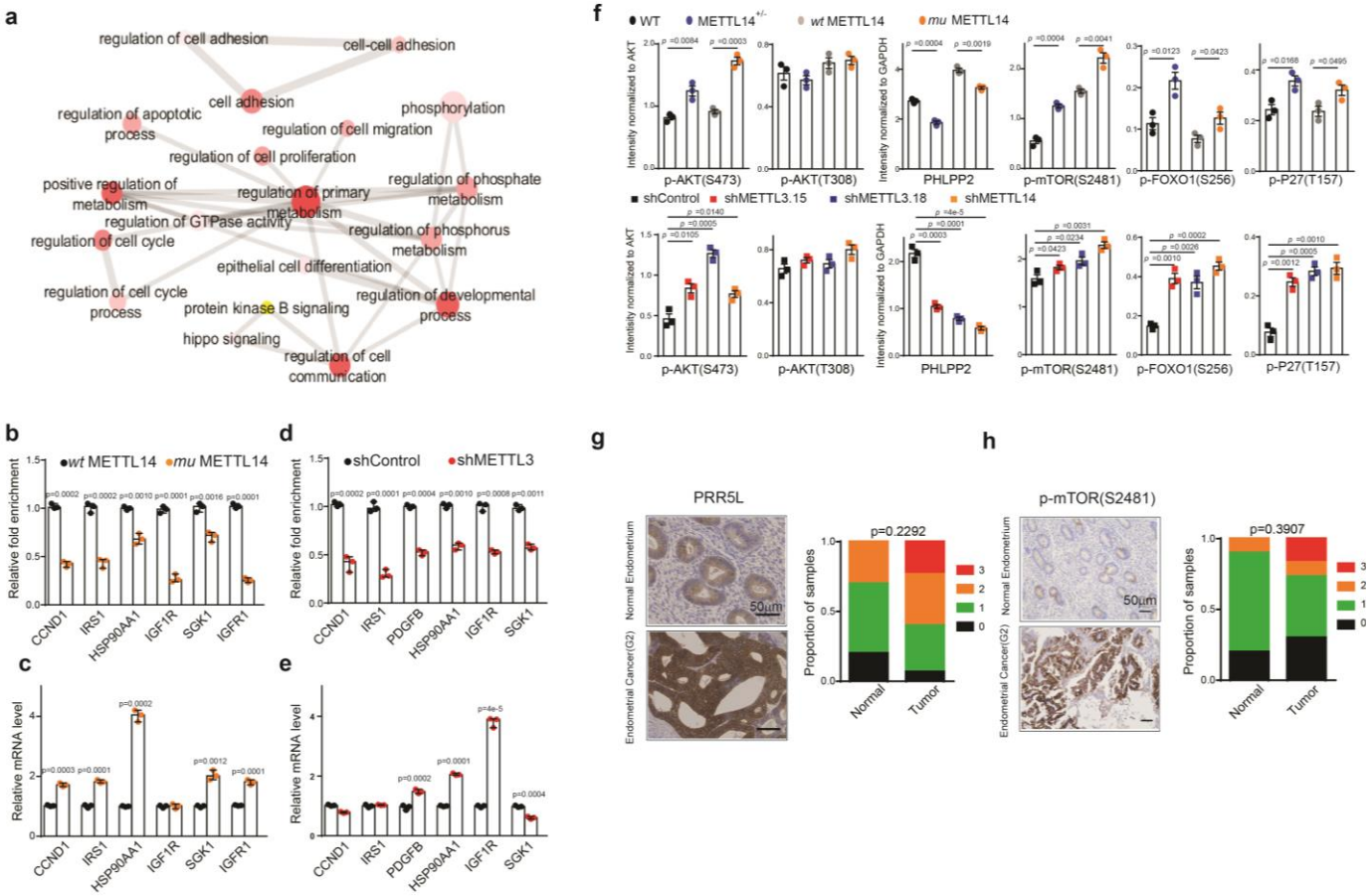

Supplementary Figure 4

GO term analysis and RT-qPCR validation for m^{6}A-seq results.

(**a**) GO term analysis of transcripts with reduced m^{6}A in knockdown METTL3 and mutant METTL14 HEC-1-A cells versus control. (**b-e**) m^{6}A IP combined with RT-qPCR was used to quantify the relative m^{6}A levels (**b,d**) and mRNA levels (**c,e**) in the METTL14 mutant cell line (**b,c**) and METTL3 knockdown cells (**d,e**) versus control. For panels b-e, error bars indicate mean ± s.e.m from *n* = 3 biological replicates. *p*-values determined by two-tailed *t*-test. (**f**) Quantification of the immunoblots in **Figs. 4a, b**. Error bars indicate mean ± s.e.m from *n* = 3 biological replicates. *p*-values determined by two-tailed *t*-test. (**g,h**) Left: Immunohistochemical staining of tissue microarray cores for PRR5L (**g**) and p-mTOR(S2481) (**h**). Right: Quantification of IHC staining in normal endometrium (*n* = 10) and endometrial tumors (*n* = 30). Staining was assessed using automated software[55] and scored on a scale of 0 (no staining) to 3 (high staining). The *p*-value was determined by a χ^2-test. Scale bar = 50μm.

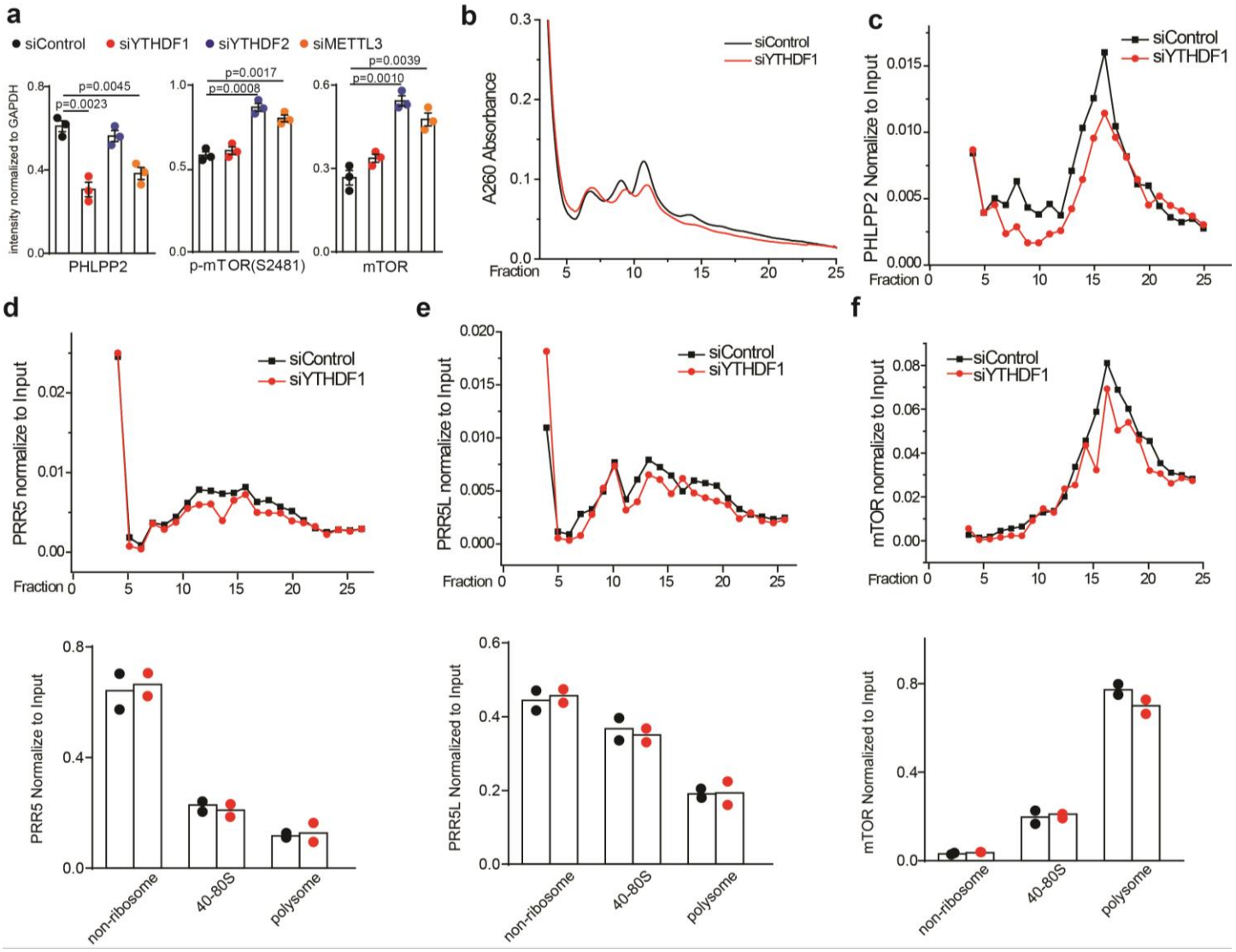

Supplementary Figure 5

Polysome profiling of m^{6}A methylated transcripts.

(**a**) Quantification of the immunoblots in **Fig. 5a**. Error bars indicate mean ± s.e.m. from *n* = 3 biological replicates. *p*-values determined by two-tailed *t*-test. (**b**) The absorbance at 260 nm was measured during fractionation of polysomes from HEC-1-A cells transiently transfected with control siRNA or siRNA targeting YTHDF1. (**c**) The abundance of *PHLPP2* transcripts was measured by RT-qPCR in each fraction from the polysome profiling. (**d-f)** Top: The abundance of *PRR5* (**d**), *PRR5L* (**e**), and *mTOR* (**f**) transcripts were measured by RT-qPCR in each fraction from the polysome profiling. Bottom: Fractions from the polysome fractionation corresponding to non-ribosomal RNAs, ribosome-associated RNAs, and polysome-associated RNAs were pooled and the abundance of the *PRR5* (**d**), *PRR5L* (**e**), and *mTOR* (**f**) transcripts were quantified by RT-qPCR. For c-f, *n* = 2 biological replicates, bar represents the mean value.

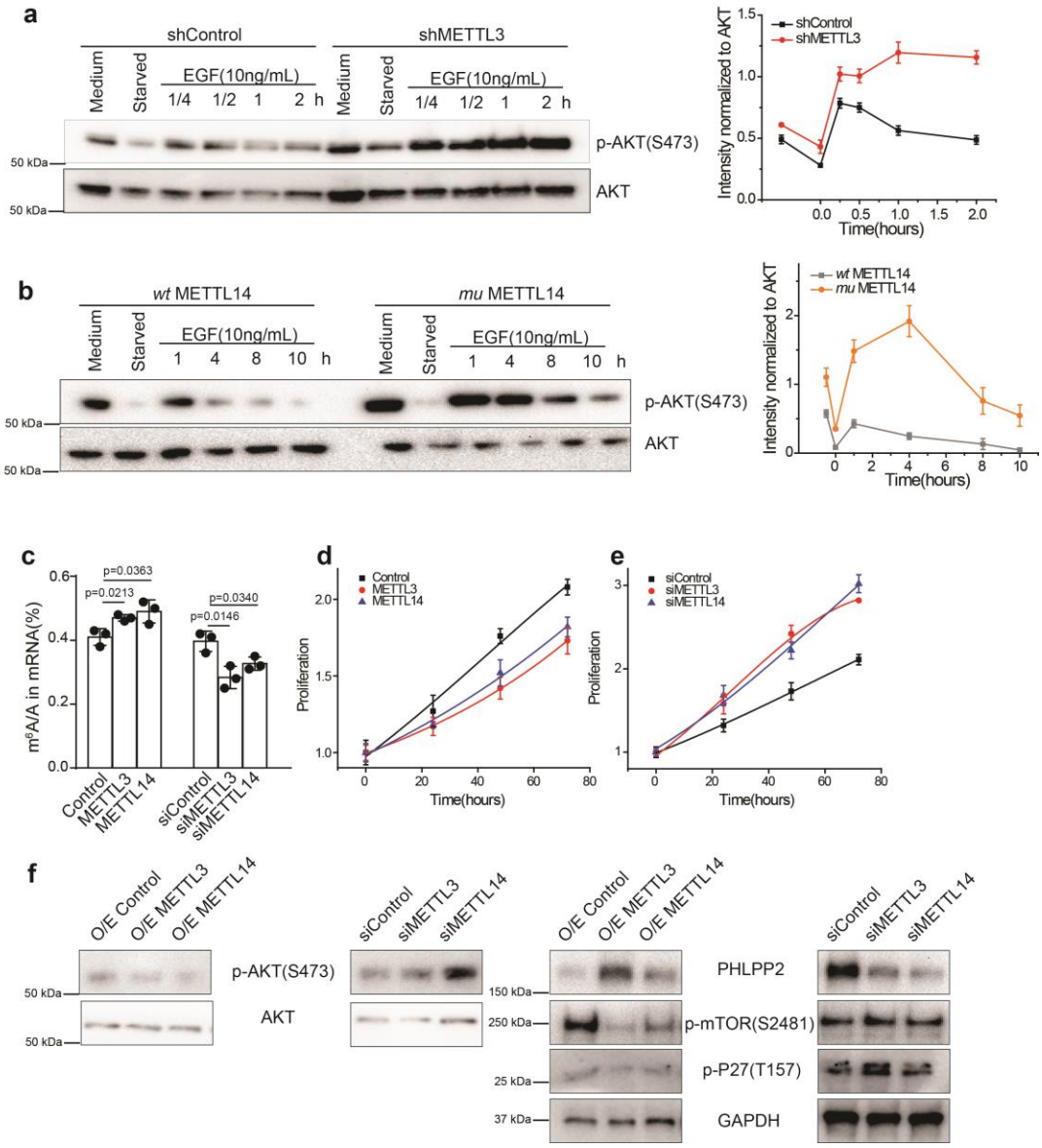

Supplementary Figure 6

Time course of AKT activation during EGF stimulation and effects of m^{6}A methylation on the RL95-2 cell line.

(**a-b**) Immunoblots showing the time course of AKT(S473) phosphorylation after EGF stimulation in shControl *versus* shMETTL3 HEC-1-A cells (**a**) or HEC-1-A cells expressing wild-type METTL14 *versus* mutant METTL14 (**b**). Cells were either incubated in media with 10% FBS (medium) or no FBS (starved). After 16 h of starvation, cells were stimulated with 10 ng/mL of recombinant EGF for the indicated amounts of time. Plots quantifying the time-course of EGF activation show mean ± s.e.m. from *n* = 3 biological replicates. *p*-values determined by two-tailed *t*-test. (**c-f**) Effects of alterations to m^{6}A methylation on RL95-2 endometrial cancer cells were examined after transient transfection with control siRNA, siRNA targeting METTL3, siRNA targeting METTL14, empty vector, plasmid encoding METTL3 or plasmid encoding METTL14. (**c**) LC-MS/MS quantification of the m^{6}A/A ratio in polyA-RNA after transient transfection of RL95-2 cells with the indicated reagents. (**d,e**) Cell proliferation measured by MTS assay of RL95-2 cells transfected with the indicated reagents. Cell numbers were normalized to the MTS signal ~ 5 h after cell seeding. For panels c-e, error bars indicate mean ± s.e.m from *n* = 3 biological replicates. *p*-values determined by two-tailed *t*-test. (**f**) Immunoblot showing the effects of the indicated perturbations to m^{6}A methylation on the expression and phosphorylation of proteins involved in the AKT pathway in RL95-2 cells. Three independent experiments have been repeated with similar results. Raw gel images for panels a, b and f are provided in **Supplementary Fig. 8**.

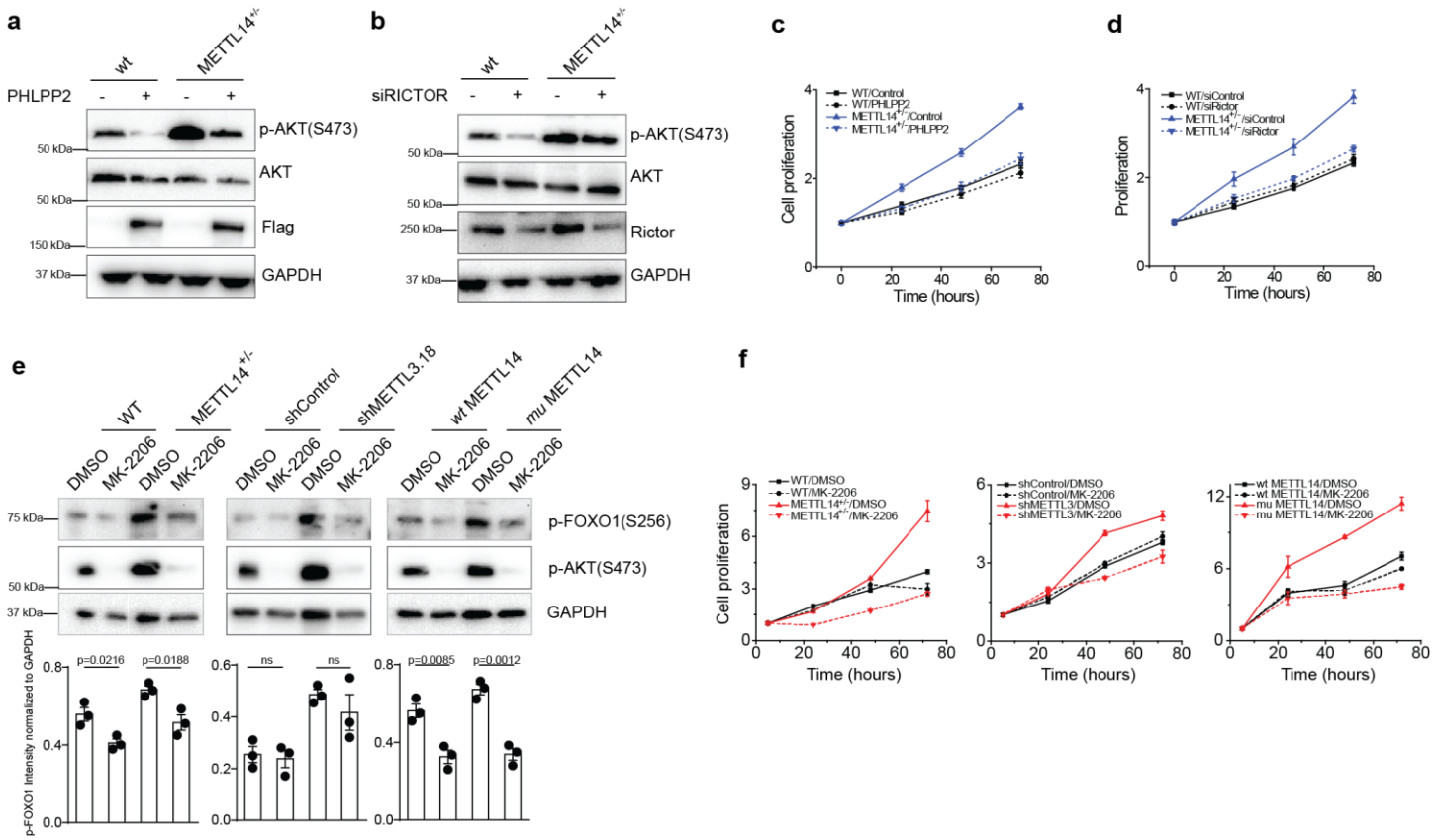

Supplementary Figure 7

Alteration of the AKT pathway rescues changes in cell proliferation due to reduced m^{6}A methylation.

(**a,b**) Immunoblots analyzing the effect of FLAG-PHLPP2 overexpression (**a**) or RICTOR knockdown (**b**) on AKT phosphorylation in wild-type and METTL14$^{+/-}$ HEC-1-A cells. Three independent experiments have been repeated with similar results. (**c-d**) Proliferation measured by MTS assay of wild-type *versus* METTL14$^{+/-}$ HEC-1-A cells. Cells were transiently transfected with a PHLPP2 overexpression plasmid *versus* empty vector (**c**) or siRNAs targeting RICTOR *versus* negative control siRNAs (**d**). Error bars show mean ± s.e.m. from *n* = 3 biological replicates. (**e**) Immunoblots showing phosphorylation status of AKT(S473) and FOXO1(S256), a downstream target of AKT, after treatment of the indicated HEC-1-A cell lines with 5μM MK-2206 for 24 h. Three independent experiments have been repeated with similar results. Plots quantifying the phosphorylation status of FOXO1(S256) show mean ± s.e.m. from *n* = 3 biological replicates. *p*-values determined by two-tailed *t*-test. (**f**) Cell proliferation measured by MTS assay for the indicated cell lines in the presence of 5μM MK-2206 or DMSO. For proliferation assays, cell numbers were normalized to the MTS signal ~ 5 h after cell seeding. *n* = 3 biological replicates; error bars indicate mean ± s.e.m. Raw gel images for panels a, b and e are provided in **Supplementary Fig. 8**.

Fig. 4a

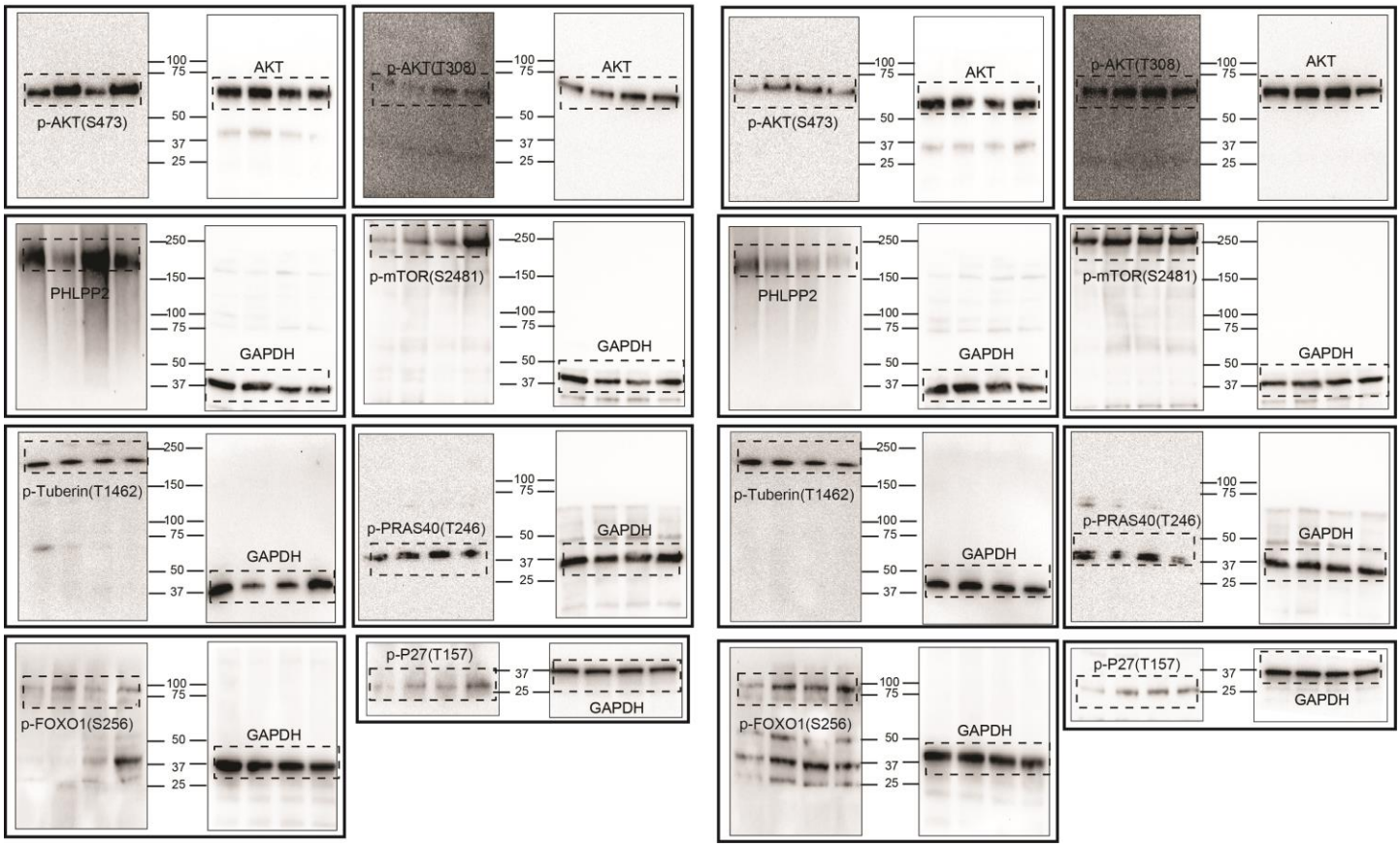

Supplementary Figure 8

Unprocessed original scans of blots.

Unprocessed images of all immunoblots. Molecular weight markers in kDa.

Fig. 5a

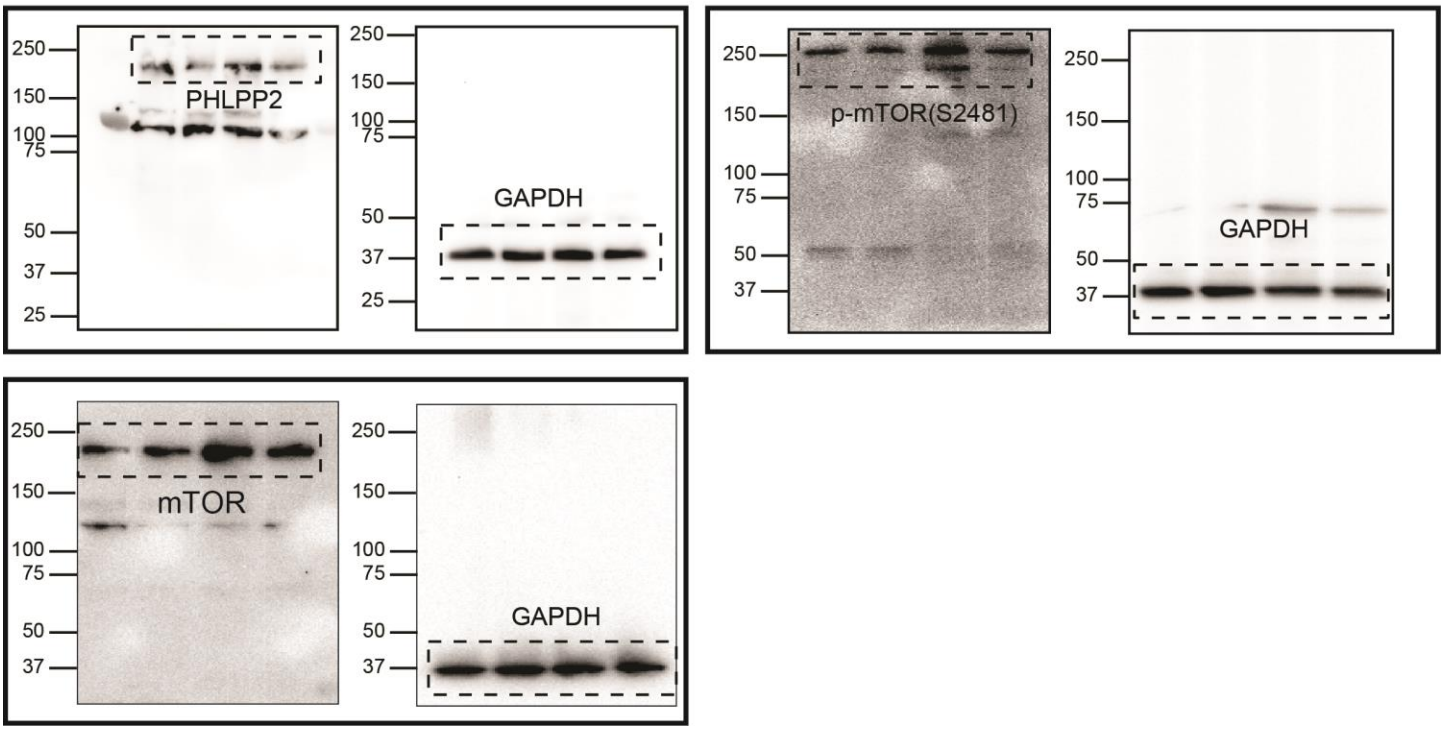

Supplementary Figure 8 Continued

Unprocessed original scans of blots.

Unprocessed images of all immunoblots. Molecular weight markers in kDa.

Fig. 6f

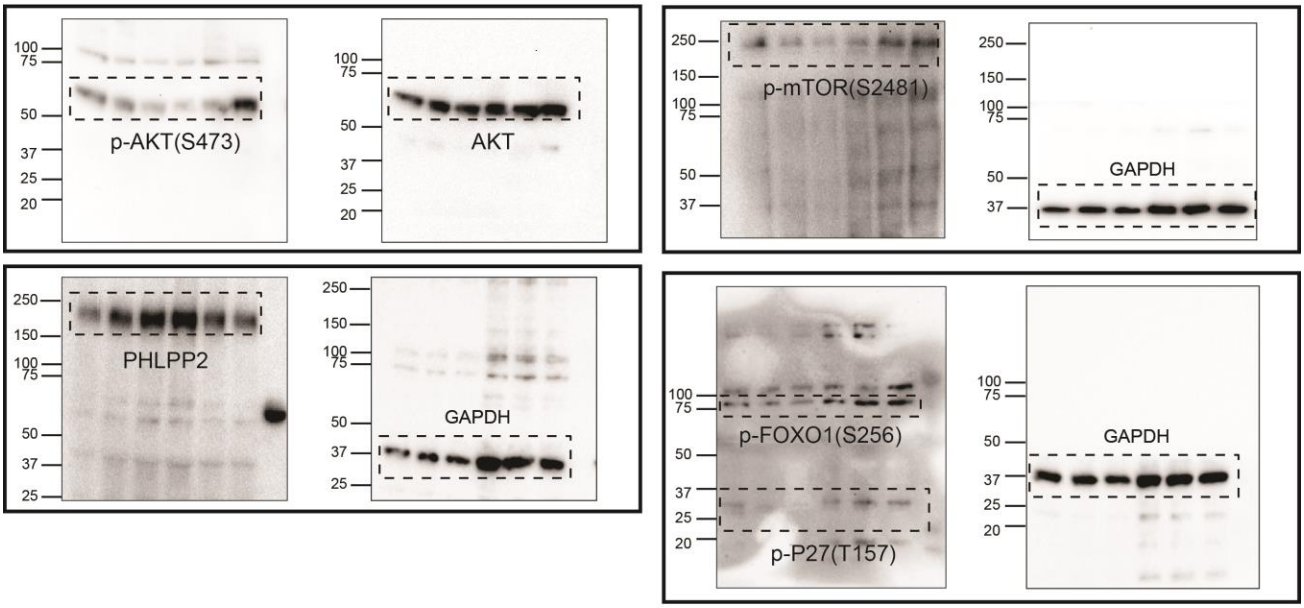

Fig. 6g

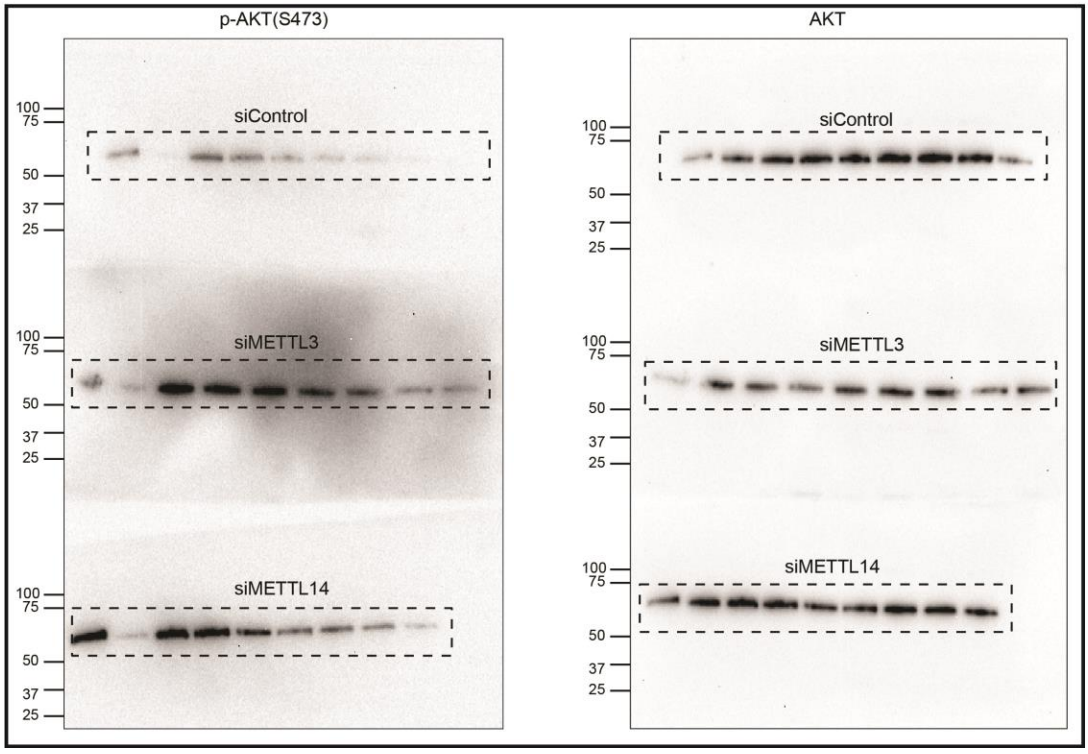

Supplementary Figure 8 Continued

Unprocessed original scans of blots.

Unprocessed images of all immunoblots. Molecular weight markers in kDa.

Fig. 7a

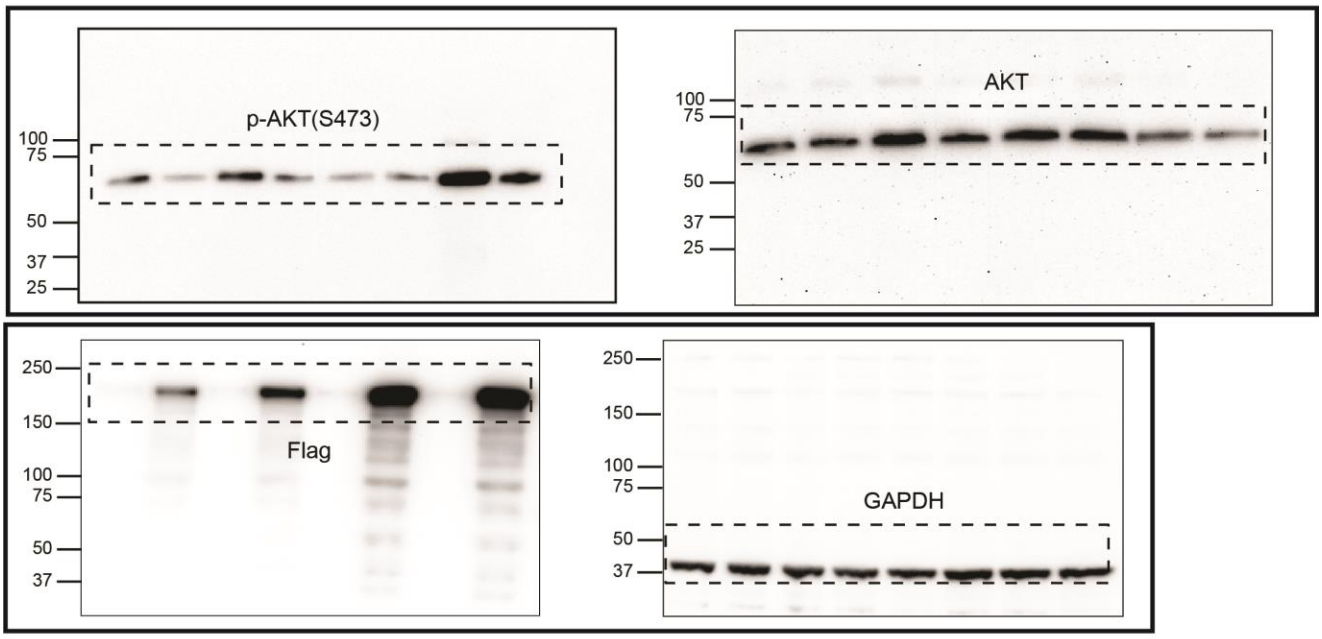

Fig. 7b

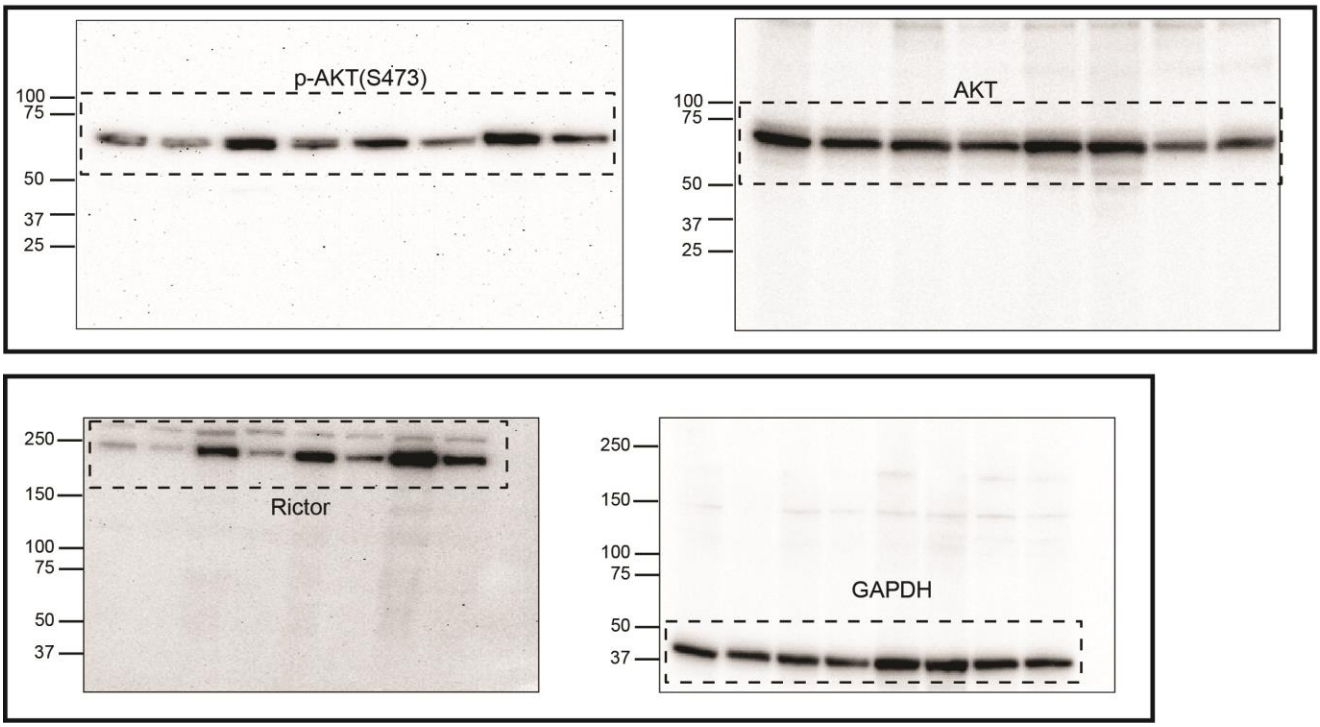

Supplementary Figure 8 Continued

Unprocessed original scans of blots.

Unprocessed images of all immunoblots. Molecular weight markers in kDa.

Supplementary Fig. 2a

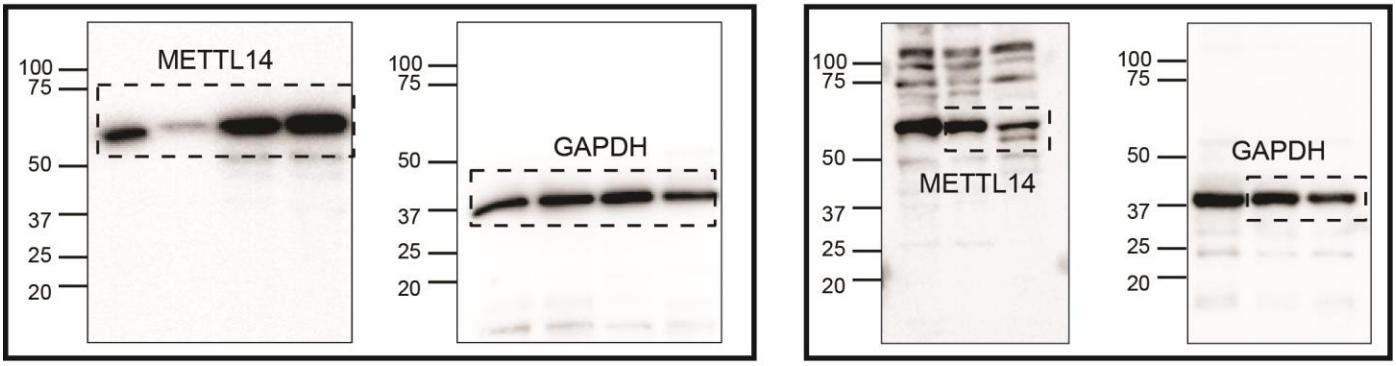

Supplementary Fig. 2i

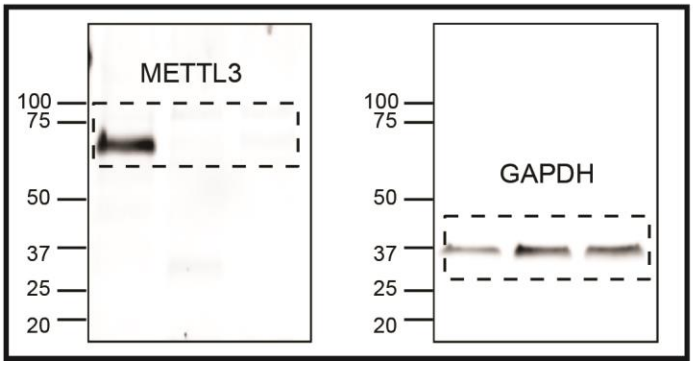

Supplementary Figure 8 Continued

Unprocessed original scans of blots.

Unprocessed images of all immunoblots. Molecular weight markers in kDa.

Supplementary Fig. 6a

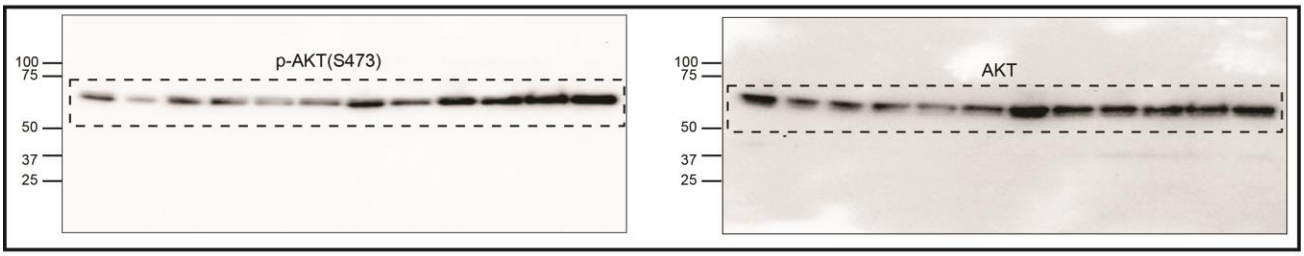

Supplementary Fig. 6b

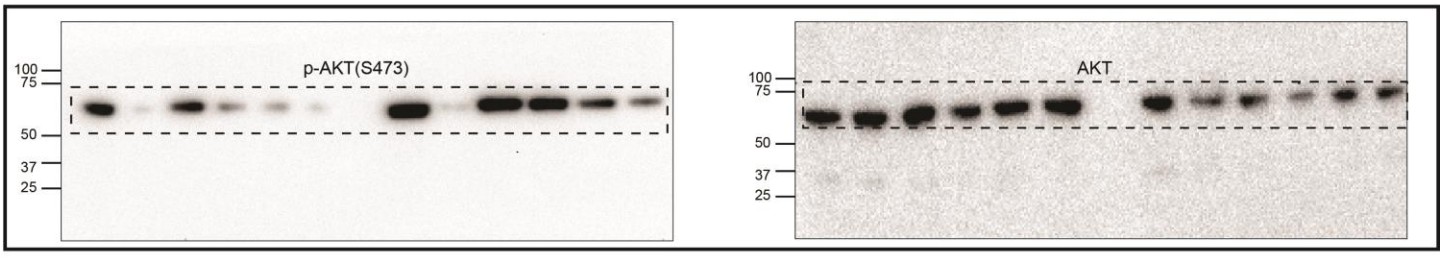

Supplementary Fig. 6f

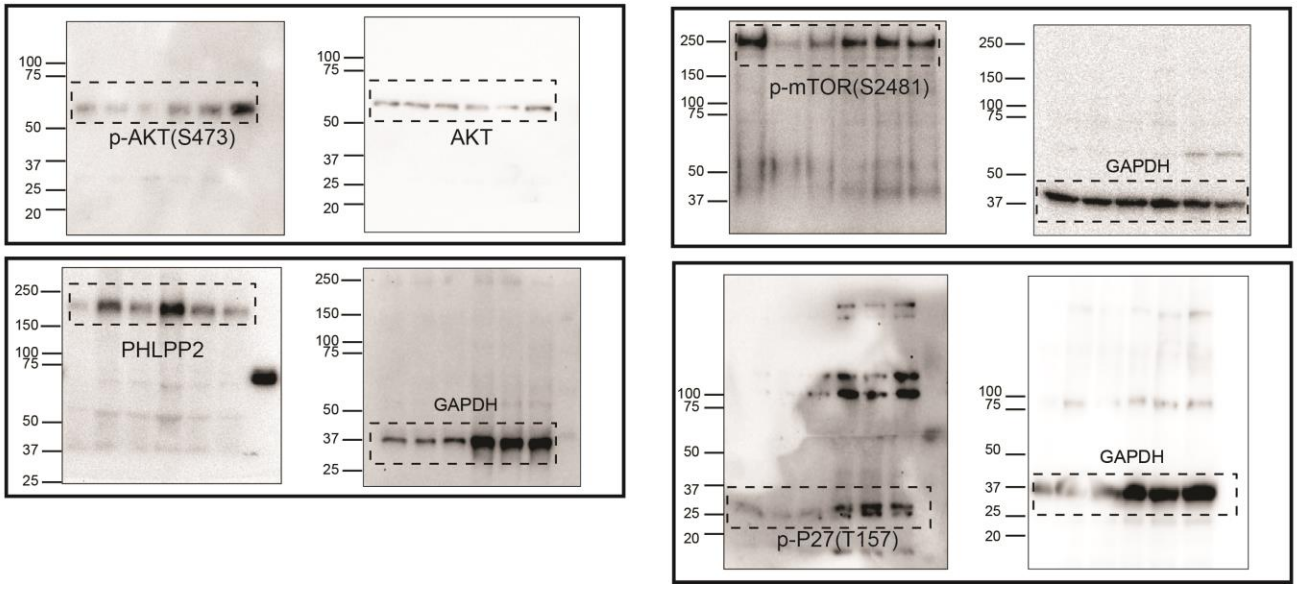

Supplementary Figure 8 Continued

Unprocessed original scans of blots.

Unprocessed images of all immunoblots. Molecular weight markers in kDa.

Supplementary Fig. 7a

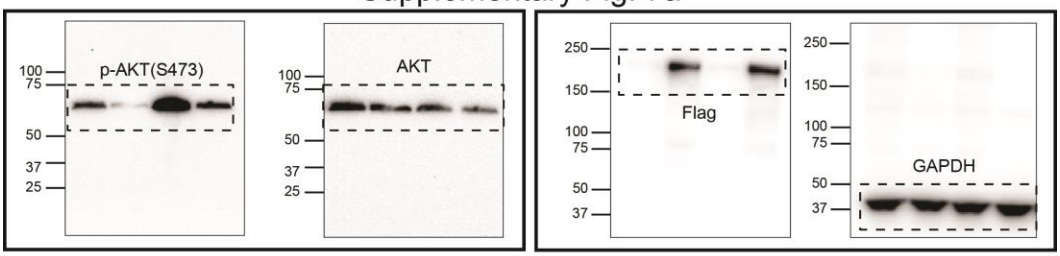

Supplementary Fig. 7b

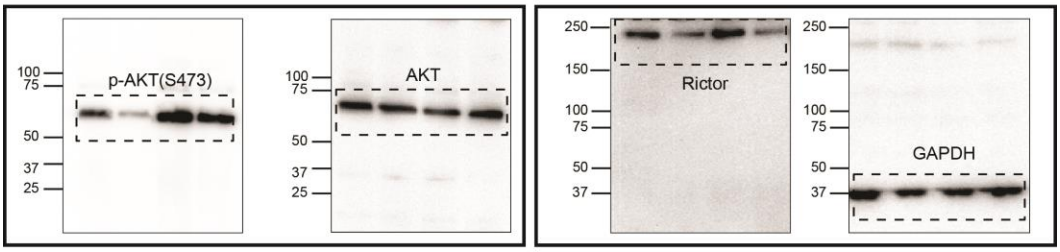

Supplementary Fig. 7e

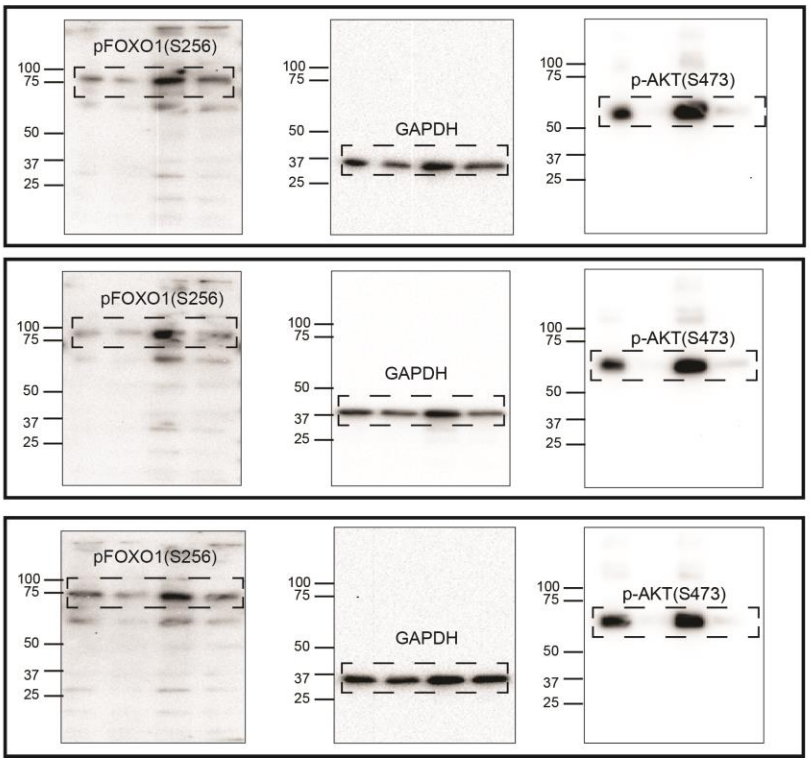

Supplementary Figure 8 Continued

Unprocessed original scans of blots.

Unprocessed images of all immunoblots. Molecular weight markers in kDa.

Supplementary Table 1 Antibody information

Supplementary Table 2 Patient sample information

Supplementary Table 3 Peaks identified from m^{6}A-seq of endometrial cancer patient samples

Supplementary Table 4 Peaks identified from m^{6}A-seq of endometrial cancer cell lines

Supplementary Table 5 Statistics Source Data